Advanced imaging and spectroscopy techniques for body magnetic resonance

Heer, P. de

1

GENERAL INTRODUCTION

INTRODUCTION

Towards High Field Body MR

Since Goldsmith et al. performed the first successful body Magnetic Resonance Imaging (MRI) scan in 1977 (Figure 1) much effort has been put into improving the (diagnostic) quality of body MR images. This improvement has been realized through enhanced gradient systems, receive/transmit coils, and pulse sequences, as well as, increased field strength of the MR systems. By increasing the field strength of the MR scanner a larger effective magnetization of the spins is produced resulting in an increase in the signal-to-noise ratio (SNR). Furthermore, with increasing field strength, the contrast of the images change, specifically when using contrast agents, creating new scanning possibilities.

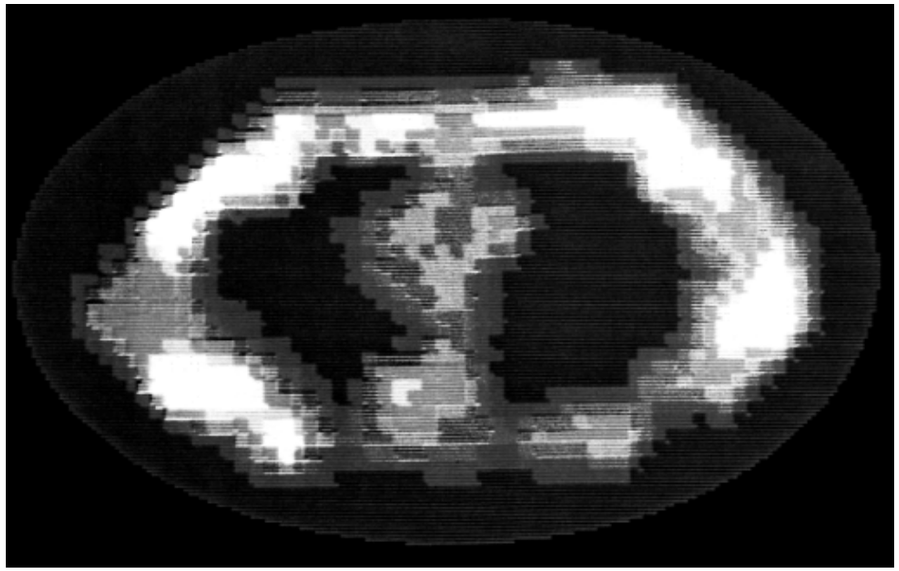

FIGURE 1: First MRI body image recorded by Goldsmith et al. By today's standards this image has an extremely low (coarse) resolution, however, basic structures like the heart and lungs are visible in the image.

High Field Advantages

In the early days, when Goldsmith recorded his first body MR image, field strengths of the scanners were well below 0.5 Tesla (T). In the following years, the field strength of clinical body MR scanners increased to 1.5 T increasing SNR and thereby improving image quality.

In the last decade, high field scanners (defined as ≥ 3 T) are increasingly used in clinical practice. High field systems are favoured over 1.5 T systems for multiple applications because of the higher SNR it provides. The additional SNR can be used to increase the resolution for imaging smaller structures (pathologies). Alternatively, the increase in SNR allows for a reduction in scan time by lowering the number of signal averages (NSA). Furthermore, high field systems can reduce acquisition time even further due to increased performance of parallel imaging methods (e.g. Spatial Encoding Using Multiple Radio Frequency Coils, SENSitivity Encoding, GeneRalized Autocalibrating Partial Parallel Acquisition) at higher field strength.[1–3] Due to the changes in contrast at higher field imaging, an increased efficacy of contrast agents, such as gadolinium (percentage T1 reduction due to gadolinium is higher), makes higher field strength more suitable for dynamic contrast enhancement (DCE) scans. Furthermore, functional neuroimaging can benefit of an increased Blood-oxygen-level dependent contrast (BOLD) response due to stronger spin-spin interaction (lower T2*) enabled by a stronger magnetic field.[4,5] In MR spectroscopy, separation of the resonance frequencies improves due to an increased chemical shift resulting in improved spectral quality and specificity.

Challenges for High Field Body MR

Despite these clear advantages of higher field scanners, clinical body imaging is still predominantly performed on 1.5 T MR scanners since the advantages previously described are not yet fully translated to clinical practice.

The main reason for this is the increase in imaging artefacts often accompanied by a higher magnetic field strength. Such artefacts are often caused by an increase in; transmit field (B_1^+) inhomogeneities (dielectric effects), static field (B_0) inhomogeneities, motion artefacts (respiratory, cardiac and bowel) and susceptibility effects. When comparing field strengths of 1.5 T and 3 T in cardiac functional imaging, Michaely et al (2006) observed only a minimal increase in SNR at 3 T.[6] Greenman et al. (2003) reported that blood suppression was comparable between 1.5 T and 3 T systems in cardiac imaging.[7] However, a decrease in SNR was found in the myocardial wall for 3 T compared to 1.5 T. This decrease in SNR was mainly attributed to the variance in the B_1^+ field. Furthermore, studies comparing 1.5 T to 3 T often report an increase in imaging artefacts.[8] Specifically artefacts caused by increased sensitivity to motion and increased magnetic susceptibility, but also B_1^+ field inhomogeneities are observed.[9,10]

Another important factor to consider when moving from 1.5 T to 3 T is that the Specific Absorption Rate (SAR) will be four times higher since this is quadratically related to the magnetic field strength.[11,12] This could complicate transferring a scan sequence from 1.5 T to 3 T since the radio frequency (RF) heating limits can be reached and changes have to be made to stay within the SAR constraints.[6]

All these challenges clearly demonstrate that it is complicated to fully exploit the theoretical advantages of higher field strengths. Additionally, the purchase and maintenance cost of high field scanners are significantly higher. Therefore, if these challenges are not addressed properly, the benefits of a higher magnetic field strength will not outweigh the higher cost.

Transmit Field (B_1^+) Variations

As mentioned in the previous paragraph, transmit field inhomogeneity is a major contributor to artefacts with increasing field strength. These artefacts represented by hyper and hypo intense areas in the image (Figure 2). This inhomogeneous B_1^+ field results in signal voids in the image and has been reported by multiple researchers.[8,13–16] As stated by Bernstein ‘‘Image shading and uneven contrast resulting from spatial variation in the transmit B_1 field remains one of the biggest unsolved problems for routine clinical 3 T imaging today”.[8] This inhomogeneity is even more prominent in patients with ascites but also in pregnant women resulting in these populations to be scanned at lower field strengths (1.5 T).

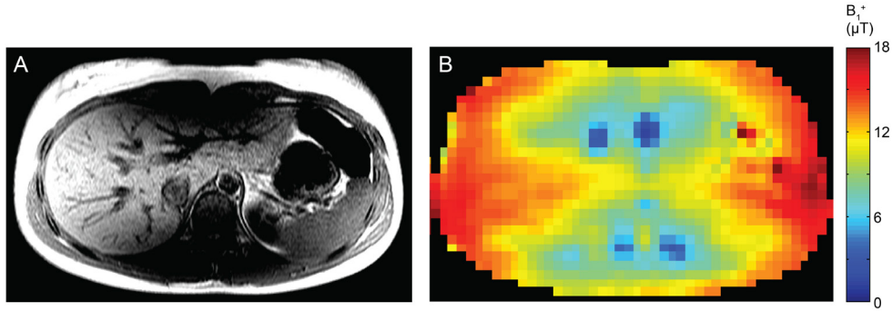

FIGURE 2: (A) T1-weighted turbo-spin echo image at 3 T with clear image hypo and hyper intensities caused by an inhomogeneous transmit field. **(B)** The corresponding transmit field map shows a low transmit field in the areas were the T1-weighted image has strong hypo intensities.

When looking at an unloaded birdcage coil the transmit field is very homogeneous for both the 1.5 and 3 T scanners. However, when a lossy object like the body is placed in the coil, the disturbance introduced by the body will cause the transmit field to be less homogeneous. This disturbance of the field is caused by a shortening of the wavelength in the body as well as attenuation of the transmit field. This is often referred to as the standing wave effect which becomes problematic when the wavelength of the transmit signal is equal or smaller than the size of the object imaged (wavelength in muscle tissue at 3 T ≈ 29cm). Both the wavelength as well as the attenuation is dependent on the field strength, with a more severe disturbance at higher field strength scanners.

MR manufacturers recognize the problem of B_1^+ inhomogeneities and are addressing it by using multi transmit set-ups. Such a multi transmit splits the standard quadrature body coil in effectively two (or more) linear transmit coils that can be independently driven with an optimized phase and amplitude. The two degrees of freedom (relative amplitudes and relative phases of the two channels) compared to only one (absolute amplitude) for a conventional single transmit system can produce considerable increases in RF transmit homogeneity [17,18] which has long been known theoretically and investigated extensively for imaging at ultra-high field (7 T).[19–21] Despite improved performance with dual-channel systems, it does not consistently solve the problem of image inhomogeneities. Experimental and simulation work has suggested that further improvement is possible using an eight channel transmit body coil, but such a setup is currently not commercially available.[22,23]

A second approach to address the issue of transmit field inhomogeneity in 3 T body imaging is the use of ''dielectric pads''.[24–27] Dielectric materials have a strong impact on the magnetic field. The extent of this effect is determined by the shape and material properties (specifically permittivity and conductivity) of these dielectrics. When a dielectric material is carefully designed it can be used to correct the inhomogeneous RF field to make it more homogeneous. Furthermore, it can increase the receive sensitivity, resulting in increased SNR. Previously these pads were made from ultrasound gel (low relative permittivity, $\mu_r < 100$) with dissolved paramagnetics, such as manganese chloride, to provide a short T2 and hence low background MR signal. Some institutions reported that such dielectric pads are used locally for most abdominal scans [25], whereas others report that they are not commonly used in the wider community.[8] Recently it was proposed that new high dielectric materials, including calcium titanate and barium titanate, would have more freedom in shaping the transmit field.[28,29] Furthermore, compared to the pads made of low permittivity materials, these pads can be made thinner which facilitates their application (Figure 3).

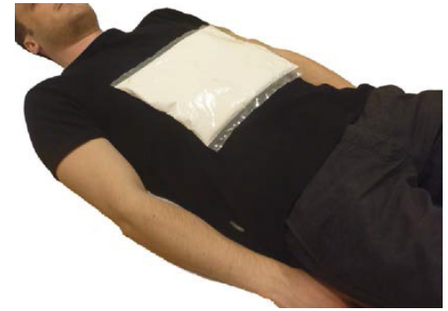

FIGURE 3: Example of a high dielectric pad placed on the liver. With this high dielectric pad it is possible to shape the transmit field to make it more homogeneous.

MR Spectroscopy

MR spectroscopy is a technique often used in research applications in body MR since it enables assessment of metabolites in the body. Instead of measuring the (water) proton densities (as in MR imaging) it is possible to measure separate metabolites and to quantify the abundance of such a metabolite. Commonly measured metabolites are triglyceride and creatine which play an important role in various diseases (e.g. metabolic syndrome and cardiovascular disease).[30–33]

However, as in MR imaging, it is challenging to translate MR spectroscopy to higher field scanners. Challenges such as an increase in transmit field (B_1^+) in-homogeneities, static field (B_0) inhomogeneities, motion artefacts (respiratory, cardiac and bowel) and susceptibility effects previously described, apply here as well. In several MR spectroscopy studies it has been shown that the potential benefits (increased SNR, better metabolite separation) are not fully utilized. For example, in brain spectroscopy a comparison between 1.5 T and 3 T Barker et al. (2001) showed an increase in SNR of only 28% and 6% of the N-acetylaspartate signal, where a gain of 100% would be expected.[34] In a second study comparing 1.5 T and 3 T spectroscopy, in both patients with mild cognitive impairment and patients with Alzheimer disease, there was no advantage in diagnostic value when using a higher field strength.[10] Both studies acclaimed the lower SNR gain to broader linewidths stressing the need for better static magnetic field (B_0) shimming methods at higher field. Another study that measured myocardial lipids showed an SNR gain of 76% for in-vivo and 45% for ex-vivo measurements, also not reaching the theoretical 100% SNR gain of doubling the scanner field strength. This suboptimal increase in SNR was also attributed to B_0 inhomogeneity as well as an increase in susceptibility and motion artefacts.[35]

Overall, body MR spectroscopy can be a challenging technique to perform specifically on high field scanners. This can also be seen from the studies that were performed to test reproducibility of the technique.[31,33,36–42] In the liver the reproducibility (coefficient of

variation) ranged from 3.6% to 10% while in the heart it ranged from 6.5% to 18%. This shows that that the reproducibility of spectroscopy varies strongly between organs but also between studies themselves. No studies evaluating the reproducibility of renal ^{1}H-MR spectroscopy for detection of renal triglyceride content had been performed prior to this thesis.

MR spectroscopy background

To understand why MR spectroscopy can be challenging to perform, specifically at high field, some background information is needed. By placing an object in a strong external magnetic field the protons in the object will align with the direction of this field. The protons will also precess (rotate around the magnetic field direction) at a frequency ω_0 that depends on the strength of the magnetic field B_0 as well as the gyromagnetic ratio γ.

$$\omega_0 = \gamma B_0 \qquad \text{(Equation 1)}$$

The gyromagnetic ratio γ is a constant and is 42.6 MHz/T for hydrogen protons. In an average clinical scanner with a field strength of 1.5 T the hydrogen protons will precess at 64 MHz. To interact with the protons in the object an RF pulse with the same frequency as the precession frequency (resonance frequency) of the protons is transmitted. The magnetization of the protons then rotates from the longitudinal plane into the transversal plane. When the RF pulse excitation ends, the magnetization of the protons will slowly return to their natural state in the direction of the applied magnetic field. During this relaxation process the object transmits a signal which can be measured by the MR scanner. By applying a Fourier transformation, the received signal is transferred from time domain into its separate frequency components.

Chemical shift

As mentioned before protons will precess at a frequency described by equation 1. However, if all protons would always precess at the same frequency we would see only one single peak in the MR spectroscopy frequency spectrum not allowing us to discriminate between different metabolites. However, the precession frequency is not solely dependent on the applied magnetic field and the gyro-magnetic ratio. There is also a third component that describes the amount of electrons surrounding (chemical environment) the protons. The electrons surrounding a proton will shield it from the external magnetic field thereby lowering the precession frequency of the proton. The effect of shielding of the electrons can be expressed in a shielding constant σ and can be applied to equation 1 to determine the effective precession frequency.

$$\omega_0 = \gamma B_0(1 - \sigma) \qquad \text{(Equation 2)}$$

The phenomena that protons experience a different magnetic field dependent on their chemical environment is called chemical shift. In MR spectroscopy we can exploit this property to discriminate between different metabolites which have different chemical environments. When an MR spectroscopy experiment is performed the received signal (after Fourier transformation) will consist of multiple peaks with each peak representing protons in a certain type of environment. Figure 4 displays an example of a liver spectrum that consists of multiple peaks that represent different metabolites. Generally, the chemical shift is expressed in parts per million (ppm) by dividing the precession frequency (in Hz) by the field strength of the scanner to create an output independent of the scanner field strength. Some structures, like triglyceride, consist of multiple moieties each with their own chemical environment and thus, resonance frequency. The most prominent resonances of triglyceride are CH_3 (0.9 ppm), $(CH_2)^n$ (1.3 ppm), $CH_2CH = CHCH_2$ and CH_2COO (2.1 ppm). By quantitatively measuring the concentrations of triglyceride in organs, assessment of cellular damage from lipotoxicity can be performed. Moreover, proton MRS enables measurement of metabolites involved in the energy supply of the body such as creatine (3 ppm). Furthermore, the amount of water (4.7 ppm) can be measured which is often used as an internal reference to quantify other metabolites.

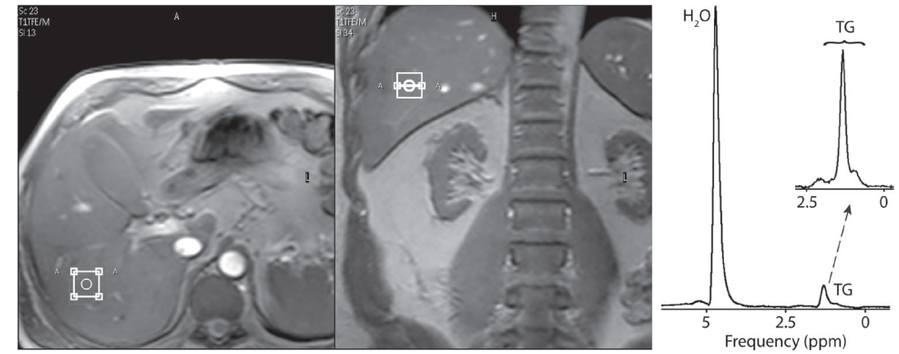

FIGURE 4: Example MR spectroscopy (single voxel) measurement in the liver with an elevated triglyceride water ratio (> 5%) compared to a healthy liver. The two images show the measurement location (white voxel) in the transverse and coronal direction. On the right the MR spectrum is shown with resonances of triglycerides (0.9, 1.3, 2.1 ppm) and water (4.7 ppm).

Even though MR spectroscopy is one of the few techniques that enables quantification of various metabolites in the body, clinical applications are currently limited to neurology, and more recently, the prostate.[43–45] Body MR spectroscopy applications are still restricted to the research domain due to the fact that it is a challenging technique to perform reliably. This is due to problems described earlier such as transmit field fluctuations, static field fluctuations as well as an inherent low SNR of the metabolites of interest.

Clinical applications of high field body MR - Metabolic Syndrome

Data of the International Diabetes Federation (IDF) shows that a quarter of the world's adult population meets the criteria for Metabolic Syndrome (MetS).[46] The IDF defined metabolic syndrome as "a cluster of the most dangerous risk factors including diabetes and prediabetes, abdominal obesity, high cholesterol and high blood pressure" increasing the risk of serious health problems like diabetes, heart failure, non-alcoholic liver disease, renal failure and stroke.[47]

- Raised plasma triglyceride level; > 150 mg/dL (> 1.7 mmol/L)
- Reduced plasma HDL cholesterol; < 40 mg/dL (1.03 mmol/L) in males and < 50 mg/dL (< 1.29 mmol/L) in females
- Raised blood pressure; systolic BP ≥ 130 or diastolic BP ≥ 85 mm Hg
- Raised fasting plasma glucose; ≥ 100 mg/dL (≥ 5.6 mmol/L)

Due to the globally increasing prevalence of obesity, as well as higher life expectancy, MetS is increasingly diagnosed as it is correlated with elevated body mass index as well as advancing age.
Although the exact underlying cause of MetS is still not fully understood, insulin resistance is considered to be a significant factor in the development of MetS. Insulin is a hormone which is produced by beta-cells in the pancreas to facilitate uptake of glucose from the blood into tissue such as liver, kidney and muscle cells. When the body becomes less sensitive to insulin, the uptake of glucose from the blood is reduced, resulting in high blood glucose levels. To compensate for these increased blood glucose levels, the beta-cells increase insulin production. This in turn increases the load on the beta-cells until the maximum insulin production is reached and glucose builds up in the blood. This effect is labelled hyperglycemia and is linked to excessive triglyceride levels in parts of the body including the liver, skeletal muscle, and heart, and renal tissue. Such raised lipids levels, described as ectopic fat deposition, interfere with cellular function and can cause cell death through a phenomena known as lipotoxicity, which plays an important role in the pathogenesis of MetS (Figure 5).[30,48]

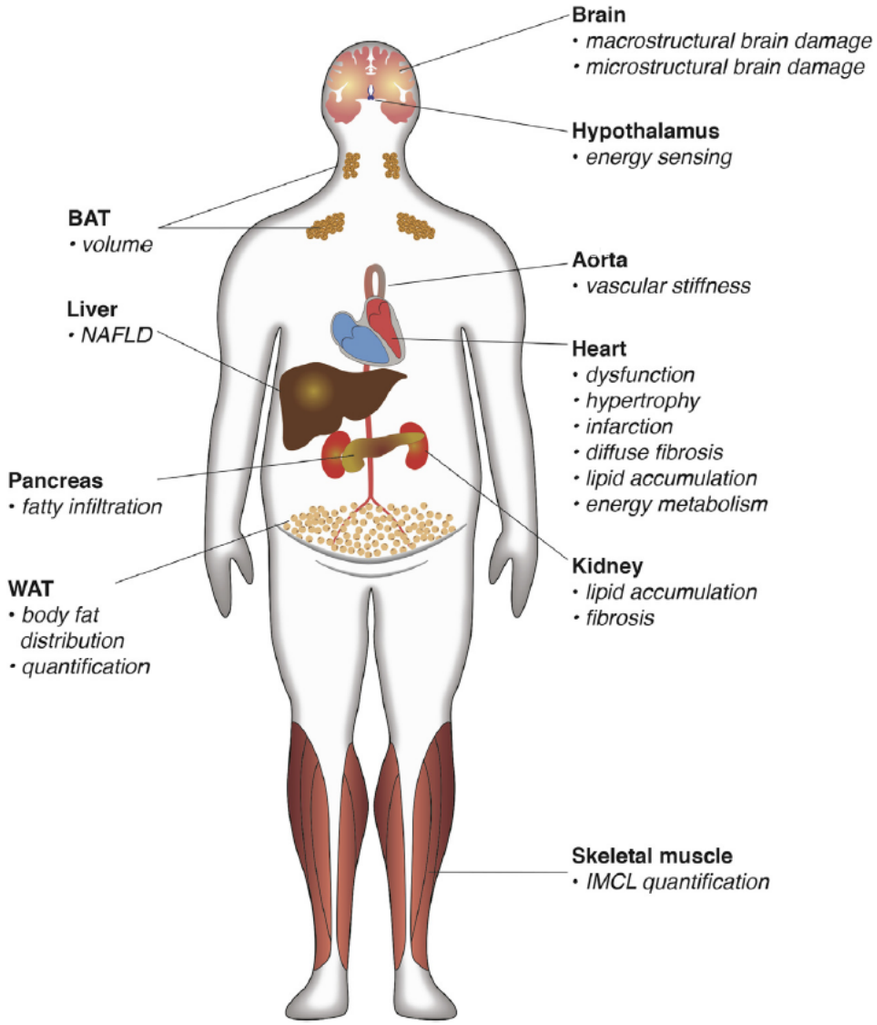

FIGURE 5: Extent of impact of metabolic syndrome that can be measured using MR. (Magnetic Resonance Imaging Clinics of North America 2015 Feb;23(1):41-58, with permission.)

Hallmarks of MetS in the heart, liver and kidney

A description of the full extent of the impact of MetS on the body is beyond the scope of this thesis and therefore, we focused on the three primarily affected organs; the heart, liver and kidney.
In the heart elevated myocardial triglyceride content has been linked to an increased chance of heart failure.[49,50] As shown in animal studies, increased storage of myocardial triglyceride reflects an abundance of toxic lipids that impair cardiomyocyte integrity and function. Myocardial steatosis may be an early sign of diabetic cardiomyopathy, because it is an independent predictor of diastolic dysfunction.
In the liver, the blood glucose is converted into glycogen or fatty acids which serve as an energy source. However, when excessive glucose is present in the blood, it will be converted to vacuoles of triglyceride lipid and stored in the liver cells. This process is called hepatic steatosis and is diagnosed in case a liver biopsy shows that more than five percent of the hepatocytes contain vacuoles of triglyceride lipid. If hepatic steatosis is not treated it can progress to non alcoholic steatotic hepatitis (NASH), characterized by inflammation of the hepatocytes. A quarter of patients with NASH develop fibrosis (scarring of the liver tissue).[51] In a subgroup of these patients, NASH eventualy results in cell death of the hepatocytes (necrosis) which often necessitates a liver transplant.
How MetS, in particular obesity, can lead to incipient chronic kidney disease remains unclear. Recently ectopic lipid accumulation in the kidney (fatty kidney) has been proposed as a potential pathway.[52–55] Notably, obesity and type 2 diabetes have been associated with renal lipid accumulation in both human and porcine kidneys with differences in anatomical distribution between glomeruli and tubuli, as well as the cortex and medulla.[53,56] Increased renal lipid content has also been linked to functional and structural renal hyperfiltration, obesity-related glomerulopathy, and type 2 diabetic nephropathy.[52,56-57]. Various rodent models have shown that intervention in cellular lipid pathways attenuated obesity-related glomerulopathy or diet-induced chronic kidney disease.[58]

At present, MetS is diagnosed by a cluster of the most dangerous risk factors. Several organizations have described such criteria (eg. IDF, WHO, ADA) and even though these diagnostic criteria are not the same they often include factors like prediabetes, abdominal obesity, high cholesterol and high blood pressure. However, these criteria provide limited information to what extent the different organs are affected. To improve treatment strategies, organ-specific (imaging) biomarkers are needed to gain more insight in the underlying mechanisms and risk stratification of MetS. Since many disease pathologies related to MetS are believed to be closely correlated to the increased storage of lipids in the organs, shown to be a precursor for lipotoxicity, a reliable technique to measure the amount of ectopic lipids in the organs is highly needed.

AIM OF THIS THESIS

The aim of this thesis is to further develop advanced body MR techniques to gain more insight in the metabolic syndrome (MetS). This was realized by optimizing MR imaging and spectroscopy measurements in the body, as well as ex-vivo. One of the optimization steps includes development of high dielectric materials to increase sensitivity of the body MR measurements.

OUTLINE OF THIS THESIS

In **Chapter one** a general introduction is given to body MR and the challenges of high field body MR are discussed. Basic background information for dielectric pads is given, which can be applied to address a major challenge of high field body MR. Moreover some basic principles of MR spectroscopy are explained. Furthermore, the metabolic syndrome and the use of high field body MR to evaluate this syndrome are described. In the first part of this thesis we aimed to develop new techniques for high field body MR which are described in chapters two, three, and four. **Chapter two** (Increasing Signal Homogeneity and Image Quality in Abdominal Imaging at 3 T with Very High Permittivity Materials) examines whether inhomogeneous transmit fields (a major challenge in high field body MR), can be improved by passive shimming. High dielectric materials were designed, simulated and tested for liver imaging to increase image quality. **Chapter three** (Improved Cardiac Proton Magnetic Resonance Spectroscopy at 3 T Using High Permittivity Pads) demonstrates how a similar passive shimming approach can be applied in cardiac spectroscopy to increase the SNR of the spectra. In **Chapter four** (Parameter Optimization for Reproducible Cardiac ^{1}H-MR Spectroscopy at 3 Tesla) we investigated how cardiac proton MR spectroscopy measurements can be optimized for high field and reports results on reproducibility. In the second part of this thesis, consisting of chapters five, six and seven, the techniques described in chapters 2, 3 and 4 are applied in clinical studies in order to gain additional insight in the development/treatment of the Metabolic Syndrome (MetS). In **Chapter five** (MR of Multi-Organ Involvement in the Metabolic Syndrome) a review is presented on multi-organ involvement in the metabolic syndrome and how this can be evaluated using magnetic resonance techniques. **Chapter six** (Metabolic Imaging of Human Kidney Triglyceride Content: Reproducibility of Proton Magnetic Resonance Spectroscopy) reports the results of a feasibility study of in-vivo renal proton MR spectroscopy and describes the reproducibility of this measurement. **Chapter seven** (Imaging Fatty Kidney by Clinical Proton Magnetic Resonance Spectroscopy (^{1}H-MRS): a First Validation and Dietary Intervention Study using Porcine Kidneys) validates renal proton MR spectroscopy in comparison to biopsies in porcine kidneys. Furthermore, the effects of dietary intervention on renal lipids are assessed. In **Chapter eight** all chapters are summarized and discussed.

REFERENCES

1. Sodickson DK, Manning WJ. Simultaneous acquisition of spatial harmonics (SMASH): Fast imaging with radiofrequency coil arrays. *Magn Reson Med*. 1997;38(4):591-603. doi:10.1002/mrm.1910380414.

2. Pruessmann KP, Weiger M, Scheidegger MB, Boesiger P. ._SENSE sensitivity encoding for fast MRI.pdf. *Magn Reson Med Off J Soc Magn Reson Med / Soc Magn Reson Med*. 1999;42(5):952-962. http://www.ncbi.nlm.nih.gov/pubmed/10542355.

3. Griswold MA, Jakob PM, Heidemann RM, et al. Generalized Autocalibrating Partially Parallel Acquisitions (GRAPPA). *Magn Reson Med*. 2002;47(6):1202-1210. doi:10.1002/mrm.10171.

4. Jesmanowicz A, Bandettini PA, Hyde JS. Single-shot half k-space high-resolution gradient-recalled EPI for fMRI at 3 Tesla. *Magn Reson Med*. 1998;40(5):754-762. doi:10.1002/mrm.1910400517.

5. Krüger G, Kastrup A, Glover GH. Neuroimaging at 1.5 T and 3.0 T: Comparison of oxygenation-sensitive magnetic resonance imaging. *Magn Reson Med*. 2001;45(4):595-604. doi:10.1002/mrm.1081.

6. Michaely HJ, Nael K, Schoenberg SO, et al. Analysis of cardiac function - Comparison between 1.5 tesla and 3.0 tesla cardiac cine magnetic resonance imaging: Preliminary experience. *Invest Radiol*. 2006;41(2):133-140. doi:10.1097/01.rli.0000192023.96494.af.

7. Greenman RL, Shirosky JE, Mulkern R V., Rofsky NM. Double inversion black-blood fast spin-echo imaging of the human heart: A comparison between 1.5T and 3.0T. *J Magn Reson Imaging*. 2003;17(6):648-655. doi:10.1002/jmri.10316.

8. Bernstein MA, Huston J, Ward HA. Imaging artifacts at 3.0T. *J Magn Reson Imaging*. 2006;24(4):735-746. doi:10.1002/jmri.20698.

9. Kuhl CK, Textor J, Gieseke J, et al. Acute and subacute ischemic stroke at high-field-strength (3.0-T) diffusion-weighted MR imaging: intraindividual comparative study. *Radiology*. 2005;234(2):509-516. doi:10.1148/radiol.2342031323.

10. Kantarci K, Reynolds G, Petersen RC, et al. Proton MR spectroscopy in mild cognitive impairment and Alzheimer disease: comparison of 1.5 and 3 T. *AJNR Am J Neuroradiol*. 2003;24(5):843-849. doi:3T Library-Converted #37; Continuum-Converted #3; Used to be #1192.

11. Collins CM, Smith MB. Signal-to-noise ratio and absorbed power as functions of main magnetic field strength, and definition of "90??" RF pulse for the head in the birdcage coil. *Magn Reson Med*. 2001;45(4):684-691. doi:10.1002/mrm.1091.

12. Vaughan JT, Garwood M, Collins CM, et al. 7T vs. 4T: RF power, homogeneity, and signal-to-noise comparison in head images. *Magn Reson Med*. 2001;46(1):24-30. doi:10.1002/mrm.1156.

13. Cornfeld D, Weinreb J. Simple changes to 1.5-T MRI abdomen and pelvis protocols to optimize results at 3 T. *AJR Am J Roentgenol*. 2008;190(2):140-150. doi:10.2214/AJR.07.2903.

14. Dietrich O, Reiser MF, Schoenberg SO. Artifacts in 3-T MRI: Physical background and reduction strategies. *Eur J Radiol*. 2008;65(1):29-35. doi:10.1016/j.ejrad.2007.11.005.

15. Yang RK, Roth CG, Ward RJ, deJesus JO, Mitchell DG. Optimizing Abdominal MR Imaging: Approaches to Common Problems. *RadioGraphics*. 2010;30(1):185-199. doi:10.1148/rg.301095076.

16. Merkle EM, Dale BM. Abdominal MRI at 3.0 T: the basics revisited. *AJR Am J Roentgenol*. 2006;186(6):1524-1532. doi:10.2214/AJR.05.0932.

17. Nelles M, König RS, Gieseke J, et al. Dual-source parallel RF transmission for clinical MR imaging of the spine at 3.0 T: intraindividual comparison with conventional single-source transmission. *Radiology*. 2010;257(3):743-753. doi:10.1148/radiol.10092146.

18. Willinek WA, Gieseke J, Kukuk GM, et al. Dual-source parallel radiofrequency excitation body MR imaging compared with standard MR imaging at 3.0 T: initial clinical experience. *Radiology*. 2010;256(3):966-975. doi:10.1148/radiol.10092127.

19. Adriany G, Van de Moortele P-F, Wiesinger F, et al. Transmit and receive transmission line arrays for 7 Tesla parallel imaging. *Magn Reson Med*. 2005;53(2):434-445. doi:10.1002/mrm.20321.

20. Vaughan JT, Snyder CJ, DelaBarre LJ, et al. Whole-body imaging at 7T: Preliminary results. *Magn Reson Med*. 2009;61(1):244-248. doi:10.1002/mrm.21751.

21. Kraff O, Bitz AK, Kruszona S, et al. An eight-channel phased array RF coil for spine MR imaging at 7 T. *Invest Radiol*. 2009;44(11):734-740. doi:10.1097/RLI.0b013e3181b24ab7.

22. Van den Berg CAT, van den Bergen B, Van de Kamer JB, et al. Simultaneous B1 + homogenization and specific absorption rate hotspot suppression using a magnetic resonance phased array transmit coil. *Magn Reson Med*. 2007;57(3):577-586. doi:10.1002/mrm.21149.

23. Vernickel P, Röschmann P, Findeklee C, et al. Eight-channel transmit/receive body MRI coil at 3T. *Magn Reson Med*. 2007;58(2):381-389. doi:10.1002/mrm.21294.

24. Franklin KM, Dale BM, Merkle EM. Improvement in B1-inhomogeneity artifacts in the abdomen at 3T MR imaging using a radiofrequency cushion. *J Magn Reson Imaging*. 2008;27(6):1443-1447. doi:10.1002/jmri.21164.

25. Sreenivas M, Lowry M, Gibbs P, Pickles M, Turnbull LW. A simple solution for reducing artefacts due to conductive and dielectric effects in clinical magnetic resonance imaging at 3T. *Eur J Radiol*. 2007;62(1):143-146. doi:10.1016/j.ejrad.2006.11.014.

26. Takayama Y, Nonaka H, Nakajima M, Obata T, Ikehira H. Reduction of a high-field dielectric artifact with homemade gel. *Magn Reson Med Sci*. 2008;7(1):37-41. http://www.ncbi.nlm.nih.gov/pubmed/18460847. Accessed August 21, 2017.

27. Kataoka M, Isoda H, Maetani Y, et al. MR imaging of the female pelvis at 3 Tesla: evaluation of image homogeneity using different dielectric pads. *J Magn Reson Imaging*. 2007;26(6):1572-1577. doi:10.1002/jmri.21173.

28. Teeuwisse WM, Brink WM, Haines KN, Webb AG. Simulations of high permittivity materials for 7 T neuroimaging and evaluation of a new barium titanate-based dielectric. *Magn Reson Med*. 2012;67(4):912-918. doi:10.1002/mrm.24176.

29. Teeuwisse WM, Brink WM, Webb AG. Quantitative assessment of the effects of high-permittivity pads in 7 Tesla MRI of the brain. *Magn Reson Med*. 2012;67(5):1285-1293. doi:10.1002/mrm.23108.

30. Iozzo P. Myocardial, perivascular, and epicardial fat. *Diabetes Care*. 2011;34 Suppl 2(Supplement_2):S371-9. doi:10.2337/dc11-s250.

31. Machann J, Stefan N, Schick F. (1)H MR spectroscopy of skeletal muscle, liver and bone marrow. *Eur J Radiol*. 2008;67(2):275-284. doi:10.1016/j.ejrad.2008.02.032.

32. Lee SS, Park SH. Radiologic evaluation of nonalcoholic fatty liver disease. *World J Gastroenterol*. 2014;20(23):7392. doi:10.3748/wjg.v20.i23.7392.

33. van der Meer RW, Doornbos J, Kozerke S, et al. Metabolic imaging of myocardial triglyceride content: reproducibility of 1H MR spectroscopy with respiratory navigator gating in volunteers. *Radiology*. 2007;245(1):251-257. doi:10.1148/radiol.2451061904.

34. Barker PB, Hearshen DO, Boska MD. Single-voxel proton MRS of the human brain at 1.5 T and 3.0 T. *Magn Reson Med*. 2001;45(5):765-769.

35. Venkatesh BA, Lima JAC, Bluemke DA, Lai S, Steenbergen C, Liu CY. MR proton spectroscopy for myocardial lipid deposition quantification: A quantitative comparison between 1.5T and 3T. *J Magn Reson Imaging*. 2012;36(5):1222-1230. doi:10.1002/jmri.23761.

36. Johnson NA, Walton DW, Sachinwalla T, et al. Noninvasive assessment of hepatic lipid composition: Advancing understanding and management of fatty liver disorders. *Hepatology*. 2008;47(5):1513-1523. doi:10.1002/hep.22220.

37. Szczepaniak LS, Nurenberg P, Leonard D, et al. Magnetic resonance spectroscopy to measure hepatic triglyceride content: prevalence of hepatic steatosis in the general population. *Am J Physiol Endocrinol Metab*. 2005;288(2):E462-8. doi:10.1152/ajpendo.00064.2004.

38. Thomas EL, Hamilton G, Patel N, et al. Hepatic triglyceride content and its relation to body adiposity: a magnetic resonance imaging and proton magnetic resonance spectroscopy study. *Gut*. 2005;54(1):122-127. doi:10.1136/gut.2003.036566.

39. van Werven JR, Hoogduin JM, Nederveen AJ, et al. Reproducibility of 3.0 Tesla magnetic resonance spectroscopy for measuring hepatic fat content. *J Magn Reson Imaging*. 2009;30(2):444-448. doi:10.1002/jmri.21837.

40. Felblinger J, Jung B, Slotboom J, Boesch C, Kreis R. Methods and reproducibility of cardiac/respiratory double-triggered (1)H-MR spectroscopy of the human heart. *Magn Reson Med*. 1999;42(5):903-910. http://www.ncbi.nlm.nih.gov/pubmed/10542349. Accessed August 24, 2017.

41. Szczepaniak LS, Dobbins RL, Metzger GJ, et al. Myocardial triglycerides and systolic function in humans: in vivo evaluation by localized proton spectroscopy and cardiac imaging. *Magn Reson Med*. 2003;49(3):417-423. doi:10.1002/mrm.10372.

42. Ith M, Stettler C, Xu J, Boesch C, Kreis R. Cardiac lipid levels show diurnal changes and long-term variations in healthy human subjects. *NMR Biomed*. 2014;27(11):1285-1292. doi:10.1002/nbm.3186.

43. Thompson J, Lawrentschuk N, Frydenberg M, Thompson L, Stricker P. The role of magnetic resonance imaging in the diagnosis and management of prostate cancer. *BJU Int*. 2013;112(S2):6-20. doi:10.1111/bju.12381.

44. Barentsz JO, Richenberg J, Clements R, et al. ESUR prostate MR guidelines 2012. *Eur Radiol*. 2012;22(4):746-757. doi:10.1007/s00330-011-2377-y.

45. van der Graaf M. In vivo magnetic resonance spectroscopy: basic methodology and clinical applications. *Eur Biophys J*. 2010;39(4):527-540. doi:10.1007/s00249-009-0517-y.

46. National Cholesterol Education Program (NCEP) Expert Panel on Detection, Evaluation and T of HBC in A (Adult TPI. Third Report of the National Cholesterol Education Program (NCEP) Expert Panel on Detection, Evaluation, and Treatment of High Blood Cholesterol in Adults (Adult Treatment Panel III) final report. *Circulation*. 2002;106(25):3143-3421. http://www.ncbi.nlm.nih.gov/pubmed/12485966. Accessed January 9, 2017.

47. IDF T. IDF Concensus Worldwide Definition of the Metabolic Syndrome. *http://www.idf.org/webdata/docs/IDF_Meta_def_final.pdf*. 2006.

48. Després J-P, Lemieux I. Abdominal obesity and metabolic syndrome. *Nature*. 2006;444(7121):881-887. doi:10.1038/nature05488.

49. van der Meer RW, Lamb HJ, Smit JWA, de Roos A. MR Imaging Evaluation of Cardiovascular Risk in Metabolic Syndrome. *Radiology*. 2012;264(1):21-37. doi:10.1148/radiol.12110772.

50. Bizino MB, Hammer S, Lamb HJ. Metabolic imaging of the human heart: clinical application of magnetic resonance spectroscopy. *Heart*. 2014;100(11):881-890. doi:10.1136/heartjnl-2012-302546.

51. Schuppan D, Schattenberg JM. Non-alcoholic steatohepatitis: Pathogenesis and novel therapeutic approaches. *J Gastroenterol Hepatol*. 2013;28:68-76. doi:10.1111/jgh.12212.

52. de Vries APJ, Ruggenenti P, Ruan XZ, et al. Fatty kidney: emerging role of ectopic lipid in obesity-related renal disease. *Lancet Diabetes Endocrinol*. 2014;2(5):417-426. doi:10.1016/S2213-8587(14)70065-8.

53. Bobulescu IA, Lotan Y, Zhang J, et al. Triglycerides in the Human Kidney Cortex: Relationship with Body Size. Norata GD, ed. *PLoS One*. 2014;9(8):e101285. doi:10.1371/journal.pone.0101285.

54. D'Agati VD, Chagnac A, de Vries APJ, et al. Obesity-related glomerulopathy: clinical and pathologic characteristics and pathogenesis. *Nat Rev Nephrol*. 2016;12(8):453-471. doi:10.1038/nrneph.2016.75.

55. Guebre-Egziabher F, Alix PM, Koppe L, et al. Ectopic lipid accumulation: A potential cause for metabolic disturbances and a contributor to the alteration of kidney function. *Biochimie*. 2013;95(11):1971-1979. doi:10.1016/j.biochi.2013.07.017.

56. Li Z, Woollard JR, Wang S, et al. Increased glomerular filtration rate in early metabolic syndrome is associated with renal adiposity and microvascular proliferation. *Am J Physiol Renal Physiol*. 2011;301(5):F1078-87. doi:10.1152/ajprenal.00333.2011.

57. Rutledge JC, Ng KF, Aung HH, Wilson DW. Role of triglyceride-rich lipoproteins in diabetic nephropathy. *Nat Rev Nephrol*. 2010;6(6):361-370. doi:10.1038/nrneph.2010.59.

58. Wang XX, Jiang T, Shen Y, et al. The farnesoid X receptor modulates renal lipid metabolism and diet-induced renal inflammation, fibrosis, and proteinuria. *Am J Physiol Renal Physiol*. 2009;297(6):F1587-96. doi:10.1152/ajprenal.00404.2009.

59. Brink WM, van der Jagt AMA, Versluis MJ, Verbist BM, Webb AG. High permittivity dielectric pads improve high spatial resolution magnetic resonance imaging of the inner ear at 7 T. *Invest Radiol*. 2014;49(5):271-277. doi:10.1097/RLI.0000000000000026.

60. Straubinger K, Schick F, Lutz O. Pulse Angle Dependence of Double-Spin-Echo Proton NMR Spectra of Citrate--Theory and Experiments. *J Magn Reson Ser B*. 1996;110:188-194. https://ac.els-cdn.com/S1064186696900291/1-s2.0-S1064186696900291-main.pdf?_tid=fc32b39c-c31f-11e7-ad30-00000aacb35d&acdnat=1509992961_1710296761d5b549ac51ecbb90245564. Accessed November 6, 2017.

61. Kreis R. Quantitative localized 'H MR spectroscopy for clinical use. *J Prog Nucl Magn Reson Spectrosc*. 1997;31:155-195. https://ac.els-cdn.com/S0079656597000149/1-s2.0-S0079656597000149-main.pdf?_tid=2d-0ce2de-c31c-11e7-ba6f-00000aacb35e&acdnat=1509991324_99dea03b2bc60aa03df3774d91c184fa. Accessed November 6, 2017.

62. Ryner LN, Ke Y, Thomas MA. Flip Angle Effects in STEAM and PRESS--Optimized versus Sinc RF Pulses. *J Magn Reson*. 1998;131:118-125. https://ac.els-cdn.com/S1090780797913331/1-s2.0-S1090780797913331-main.pdf?_tid=d813bf3a-c31d-11e7-a7f0-00000aab0f27&acdnat=1509992041_c5d5b005b902da08bd5edeaf15216ab9. Accessed November 6, 2017.

63. Tal A, Gonen O. Spectroscopic localization by simultaneous acquisition of the double-spin and stimulated echoes. *Magn Reson Med*. 2015;73(1):31-43. doi:10.1002/mrm.25112.

64. Moonen CT, von Kienlin M, van Zijl PC, et al. Comparison of single-shot localization methods (STEAM and PRESS) for in vivo proton NMR spectroscopy. *NMR Biomed*. 1989;2(5-6):201-208. http://www.ncbi.nlm.nih.gov/pubmed/2641894. Accessed November 6, 2017.

65. Fuss TL, Cheng LL. Evaluation of Cancer Metabolomics Using ex vivo High Resolution Magic Angle Spinning (HRMAS) Magnetic Resonance Spectroscopy (MRS). *Metabolites*. 2016;6(1):11. doi:10.3390/metabo6010011.

66. Ulmer S, Backens M, Ahlhelm FJ. Basic Principles and Clinical Applications of Magnetic Resonance Spectroscopy in Neuroradiology. *J Comput Assist Tomogr*. 2016;40(1):1-13. doi:10.1097/RCT.0000000000000322.

67. in 't Zandt H, van Der Graaf M, Heerschap A. Common processing of in vivo MR spectra. *NMR Biomed*. 2001;14(4):224-232. http://www.ncbi.nlm.nih.gov/pubmed/11410940. Accessed August 24, 2017.

68. Drost DJ, Riddle WR, Clarke GD, AAPM MR Task Group #9. Proton magnetic resonance spectroscopy in the brain: report of AAPM MR Task Group #9. *Med Phys*. 2002;29(9):2177-2197. doi:10.1118/1.1501822.